

Analysis of Stresses and Strains in Geomembrane Gas Bubbles That Occur in Surface Impoundments

Richard Thiel, M. ASCE, PE¹

¹President, Thiel Engineering, PO Box 1010, Oregon House, CA 95962 richard@rthiel.com

ABSTRACT: Surface impoundments (aka, ponds) lined with geomembranes are susceptible to geomembrane uplift caused by trapped gases below the liner. This paper provides a method to analyze the shape, internal pressure, stresses, and strains in a geomembrane bubble (also called “Whales” or “Hippos”) whose pressure is caused by the gases and surrounding impounded fluid.

INTRODUCTION

Many ponds are lined with geomembranes that are not ballasted. Unballasted geomembranes are susceptible to uplift by gas pressures from below. The origin of gases below geomembranes can include air that is initially trapped below the geomembrane during installation, air in the soil that is moved upwards as a result of rising ground water, gases generated by decomposition of organic materials existing in the subgrade, or gases caused by chemical and organic reactions of fluids that leak from the pond through defects in the geomembrane. If the gases below the geomembrane are not vented, then gas bubbles often form beneath the geomembrane. They have been reported as a problem in the literature for over 30 years (e.g. Giroud and Goldstein, 1982). Specific problems that occur due to these bubbles include a) the loss of effective pond volume above the geomembrane, b) opening up of greater areas of subgrade infiltration to leakage that may occur through defects in the geomembrane, c) increased susceptibility of the geomembrane to mechanical damage caused by raising the geomembrane closer to or above the pond liquid surface, and d) debilitating stretching of the geomembrane due to the stresses and strains caused by the gas pressure, even to the point of bursting the geomembrane.

Outside of presenting bubbles as a problem, and offering general design advice to provide pond-bottom slope and subgrade venting, the author is not aware of any specific methods of quantitative analysis to address geomembrane gas bubbles. Such analyses would be valuable to understand the stresses and strains that might be caused by gas bubbles, and to provide more understanding of the bubble mechanics so that engineering design solutions can be optimized rather than guessed.

The work presented in this paper attempts to quantify the size, shape, and pressure of a gas bubble in a geomembrane where the pressure is entirely caused by the external static liquid forces in the pond on the outside of the bubble. The source of the air or gas is inconsequential to this analysis.

GEOMETRY

The assumed geometry of a bubble in the pond, surrounded by a liquid of depth H , is shown in Figure 1. This geometry is different than the standard laboratory multiaxial test (e.g. ASTM D5617) because the bottom perimeter of the bubble in a pond is not hard-clamped, but is shown with a reverse-curvature, with a point-of-inflection (POI) located a distance n above the pond bottom. The depth of the POI below the pond liquid level, given by the quantity $H-n$, is not initially known, but will be calculated.

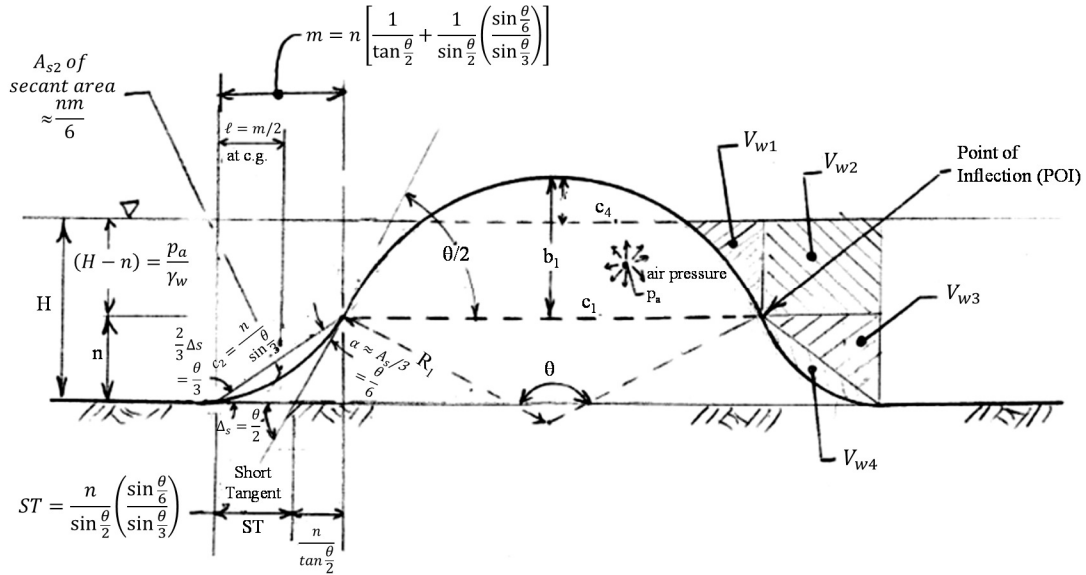


Figure 1. Bubble geometry.

The top of the pond bubble is assumed to be circular. This circular geometry, at least for the portion of the bubble above the water surface, has been shown to exist in laboratory testing, and has been observed in field situations, and would be expected for a membrane that is uniformly pressurized and symmetrically held (Bray and Merry, 1999). For purposes of the derivations developed herein, the upper portion of the bubble above the POI will be assumed to have a uniform radius, R_1 , and the diameter at the POI will be labeled c_1 . The central angle of the portion of the bubble above the POI is labeled θ (generally expressed in radians for purposes of the calculations), and thus the angle of deflection of the bubble at the POI would be $\theta/2$. By definition the arc length of the bubble above c_1 is equal to $R_1 \cdot \theta$. The height of the bubble above the POI is defined as b_1 , and is found by geometry of circles to be:

$$b_1 = R_1(1 - \cos \frac{\theta}{2}) \tag{1}$$

The average longitudinal strain, ϵ_l , of the upper portion of the bubble is classically considered in literature related to multiaxial testing (e.g. ASTM D5617) to be the difference between the arc length and the chord length, divided by the chord length, as

$$\epsilon_l = \frac{(R_1\theta - c_1)}{c_1} \tag{2}$$

This assumption for the multiaxial strain in a real-world bubble is only an approximation, and is discussed later in the paper.

If the POI is $H-n$ below the water surface, which is always the case, as proven later, then the height of the bubble that is visible above the water surface is denoted b_4 , and is given by

$$b_4 = b_1 - (H - n) \quad (3)$$

The diameter of the bubble that is visible at the water surface, c_4 , is given from the geometry of circles by:

$$c_4 = 2\sqrt{2b_4R_1 - b_4^2} \quad (4)$$

For the portion of the bubble below the POI, it is logical that the geomembrane would experience a reverse curvature that would eventually become tangent to the pond floor. Since the base of the bubble is not hard-clamped as it is in most laboratory tests, the curvature would be more gentle and with a smoother transition than in the laboratory-clamped case. The questions related to the shape of the bubble curvature below the water surface are: a) what type of curvature would exist below the water level, and b) how can the location of the POI be estimated? To answer these questions we can begin by considering the force equilibrium in a free-body diagram of a very small element of the bubble surface, as illustrated in Figure 2.

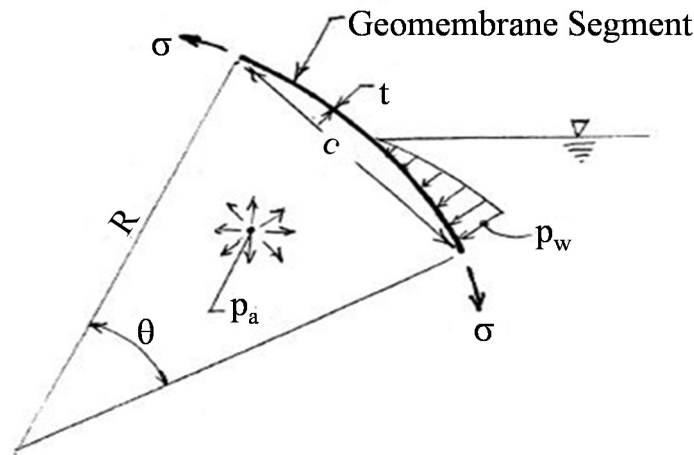


Figure 2. Stresses on small segment of bubble at water line.

On a very small segment of a portion of the bubble, the surface could approximately be assumed to have a circular curvature. That is to say, for example, that if the actual curvature is a spiral or exponential relation, it can very approximately be considered to be circular on a small localized basis. The forces on this bubble segment include the internal air pressure, p_a , which is considered constant everywhere inside the bubble; the external water pressure, p_w , which increases linearly with depth, and the geomembrane tensile stress, σ , which is assumed to be equal on both ends of the segment under consideration. Using the geometric relations of a pressurized membrane segment with a radius of curvature R , central angle θ , chord length c , thickness t , experiencing a net pressure p equal to the difference

between p_w and p_a , the force equilibrium of the segment is well documented (e.g. ASTM D5617) as:

$$\sigma = \frac{cp}{4t \sin \frac{\theta}{2}} = \frac{c(p_w - p_a)}{4t \sin \frac{\theta}{2}} \quad (5)$$

Noting from geometry that:

$$R = \frac{c}{2 \sin \frac{\theta}{2}} \quad (6)$$

then

$$\sigma = \frac{R \cdot (p_w - p_a)}{2t} \quad (7)$$

Solving for R we find:

$$R = \frac{2t\sigma}{(p_w - p_a)} \quad (8)$$

There are two significant implications of Equation (8). The first implication is that when $p_a = p_w$, then the radius of curvature R will tend towards infinity. When R is infinity, there is no curvature, and this would be the POI. Thus, the POI will exist where

$$p_a = (H-n) \cdot \gamma_w \quad (9)$$

where γ_w is the unit weight of the surrounding liquid, in this case assumed to be water. This conclusion is somewhat intuitive and makes sense.

The second implication of Equation (8) is that the radius of curvature below the water level will vary linearly with the depth below the POI. The type of curve whose radius of curvature varies linearly with the length along the curve is a clothoidal spiral. While a linear variation of curvature with the depth of liquid is not exactly the same thing as a linear variation with the length along the curve, the relationship is close enough to use as a first approximation for purposes of assigning a mathematical model for the shape of the curvature. We note that a clothoidal spiral is the type of spiral used by civil engineers for horizontal transition curves on highways and railroads, and thus the mathematics of clothoidal spirals has been developed in the profession.

There is also a third implication of Equation (8), which is that the zone of the bubble between the water surface and the POI will not be circular, and probably also has a transition curvature that would be better modeled as a clothoidal spiral. As a first approximation, and for purposes of simplifying the mathematics in this paper, this zone is considered to be circular and of the same radius as the portion of the bubble above the water surface. In other words, the portion of the bubble above c_1 is assumed to be a section of a circle of radius R_1 and central angle θ .

It will be needed to describe the strain of the upper portion of the bubble, ε_1 , solely as a function of the central angle θ . Combining Eqns (2) and (6) and solving for strain we have:

$$\varepsilon_1 = \frac{\theta}{2 \sin \frac{\theta}{2}} - 1 \quad (10)$$

Geometrical relationships for the lower portion of the bubble (see Figure 1), which is assumed to have a clothoidal spiral shape, include the following:

- Deflection angle, Δ , of the spiral, which in this case = $\theta/2$.

- Angle α that the spiral chord makes with the tangent to the POI. It is commonly accepted in civil engineering, for clothoidal spirals, that $\alpha \approx \Delta_s/3 = \theta/6$. (The basis of this assumption can be found in many standard civil engineering books. A reference used by the author is Coan, 2005.)
- The chord length of the spiral, c_2 , from trigonometry:

$$c_2 = \frac{n}{\sin \frac{\theta}{3}} \quad (11)$$

- “Short tangent length” of the spiral, ST , from triangular formula:

$$ST = \frac{n}{\sin \frac{\theta}{2}} \left(\frac{\sin \frac{\theta}{6}}{\sin \frac{\theta}{3}} \right) \quad (12)$$

- Horizontal distance m of spiral from POI to tangent with pond bottom:

$$m = ST + \frac{n}{\tan \frac{\theta}{2}} = \frac{n}{\tan \frac{\theta}{2}} + \frac{n}{\sin \frac{\theta}{2}} \left(\frac{\sin \frac{\theta}{6}}{\sin \frac{\theta}{3}} \right) \quad (13)$$

- Area of segment A_{s2} between the spiral and its chord is approximated from published equivalent area between a parabolic curve and a secant (AISC):

$$A_{s2} \cong \frac{nm}{6} \quad (14)$$

- Distance l from the lower tangent edge of the bubble to the centroid of A_{s2} is estimated, also using the properties of the secant-area of a parabola, as being half of the distance m , so that $l \approx m/2$.

The mathematics of the solution for the static forces and pressures acting on the bubble are based on summing forces in the vertical direction to achieve equilibrium for the assumed bubble shapes. To perform the analysis, certain geometric parameters must be assumed as a starting point. In the approach developed herein, the following starting parameters must be assumed:

- Unit weight of surrounding fluid, herein assumed to be water and labeled γ_w .
- Height H of water depth – with limitation that it is not above the top of the bubble.
- Thickness, t , of geomembrane.
- Chord distance c_1 of the upper bubble, which is varied for the sensitivity analyses. (Note that for the observer, only the chord c_4 is visible above the water line.)
- Central angle θ , which is varied by the investigator primarily to induce a desired strain level in the upper section of the bubble.

The method also requires an initial estimate of the height “ n ”, which is the level of the assumed inflection point, measured from the bottom of the pond. This defines the boundary at the chord c_1 which divides the “upper” bubble from the “lower” portion of the bubble, and is the location of the POI. This value is initially assumed to be equal to the water depth, H , and is then calculated iteratively to a more exact value.

Using these initial input parameters, the dimensions of the other elements of the bubble can be calculated using the geometric relationships previously described. Knowing all the dimensions of the bubble and the liquid depth, the vertical weight of the liquid that is overlying the bubble can be calculated. To perform this calculation, the liquid above the bubble is divided into four sectors as shown in Figure 1. The volume in sector 1, V_{w1} , is defined as the area of the spandrel vertically above the bubble from the POI, times the circumference of its center-of-gravity around the bubble. The formula for this is (derivation not shown due to space limitations):

$$V_{w1} = \pi(H - n) \left[c_1 - \frac{1}{24}(3c_4^2 + 3c_1^2 + 4(H - n)^2) \right] \quad (15)$$

The volume in sector 2, V_{w2} , is defined as the rectangular area next to the outside of sector 1, out to the vertical projection of the maximum radius where the lower bubble becomes tangent with the pond floor, times the circumference of its center-of-gravity around the bubble. The formula for this is:

$$V_{w2} = \pi(H - n)(m)(c_1 + m) \quad (16)$$

The volume in sector 3, V_{w3} , is defined as the right-triangular area below sector 2, whose hypotenuse is the chord of the lower-bubble spiral, times the circumference of its center-of-gravity around the bubble. The formula for this is:

$$V_{w3} = 2\pi \left[\left(\frac{c_1}{2} + m \right) - \frac{m}{3} \right] \left(\frac{m \cdot n}{2} \right) \quad (17)$$

The volume in sector 4, V_{w4} , is defined as the secant-area of the lower-bubble spiral, which is between the hypotenuse of sector 3 and the lower-bubble spiral, times the circumference of its center-of-gravity around the bubble. The formula for this is:

$$V_{w4} = \left(\frac{n \cdot m}{6} \right) \left[2\pi \left(\frac{c_1}{2} + m - l \right) \right] = \pi \left(\frac{n \cdot m}{6} \right) (c_1 + m) \quad (18)$$

Vertical equilibrium would balance the weight of the water above the bubble by the vertical force component of the pressure inside the bubble. This could be written as:

$$\gamma_w \sum_{i=1}^{i=4} V_{wi} = \frac{\pi}{4} (c_1 + 2m)^2 \cdot p_a \quad (19)$$

Where p_a is the internal air (or other gas) pressure, which can be solved as:

$$p_a = \frac{4\gamma_w}{\pi(c_1 + 2m)^2} \cdot \sum_{i=1}^{i=4} V_{wi} \quad (20)$$

Initially p_a is estimated assuming that $n=H$. Based on this preliminary estimate of p_a a revised value for n can be calculated by setting the water pressure equal to the internal gas pressure at the location of n . Thus from Eqn (9):

$$n = H - \frac{p_a}{\gamma_w} \quad (21)$$

Having a new value for n will change the geometry of the bubble, and result in a revised estimate of p_a . More iterations can be performed until the values of n and p_a stabilize.

Once p_a is known, then the value for the stress in the geomembrane in the upper portion of the bubble can be calculated using the classical Eqn (5) for the upper part of the bubble. Note that Bray and Merry (1999), and others referenced in their paper, consider the stress calculation based on Eqn (5) to be a “nominal value”. They provide other more precise equations for the “average true geomembrane stress”, or another more precise equation for the “isotropic biaxial stress at the pole”. While their alternative equations may be more precise for certain purposes, the current author notes that the field situation has many influences, primarily related to initial slack and strain distribution, such that use of the “nominal stress” formula is assumed to provide the appropriate level of accuracy and precision for this analysis.

The resulting stress and strain from the above calculations is initially somewhat arbitrary, and is dependent on the assumed geometry. The specific solution for a particular geomembrane material would be the challenge of matching the calculated multiaxial stress and strain in the bubble to the material properties of the desired geomembrane. This is done

by iteratively changing geometric parameters of the bubble shape until the stress and strain match the actual material properties. The author suggests that this analysis should be performed for the upper portion of the bubble.

EXAMPLE

Consider a bubble in an exposed 1.5 mm HDPE geomembrane pond liner that has an assumed diameter of 10 m for the upper circular portion of the bubble and is at a critical strain of 12.4%. Find the critical depth of water, H_{crit} , that will cause the stress in the geomembrane to be approximately 10,000 kPa, which matches the assumed critical strain based on the most conservative very-slow-strain multi-axial test curve (pressurized at a rate of 6.9 kPa/day) published by Nobert (1993).

Solution: STEP 1. From Eqn (10) we can calculate, for the prescribed critical strain $\varepsilon=0.124$, that the internal angle θ must be 1.658 radians (95 degrees), and from Eqn (6) that the radius of the upper portion of the bubble is

$$R_1 = \frac{10}{2 \sin\left(\frac{1.658}{2}\right)} = 6.78 \text{ m}$$

STEP 2. We can take an initial guess that the critical liquid depth $H = 1.3$ m, and that $n = H$. Taking this as a starting point, we can now calculate other bubble geometric parameters b_1 , b_4 , c_4 , and m from Eqns (1), (3), (4), and (13), respectively.

$$b_1 = 6.78\left(1 - \cos\frac{1.658}{2}\right) = 2.2 \text{ m}$$

$$b_4 = 2.2 - (1.3 - 1.3) = 2.2 \text{ m}$$

$$c_4 = 2\sqrt{2(2.2)(6.78) - 2.2^2} = 10 \text{ m}$$

$$m = \frac{1.3}{\tan\frac{1.658}{2}} + \frac{1.3}{\sin\frac{1.658}{2}} \left(\frac{\sin\frac{1.658}{6}}{\sin\frac{1.658}{3}}\right) = 2.11 \text{ m}$$

Note that in this case, since $n=H$, it makes sense that $b_1 = b_4$, and that $c_1 = c_4$.

STEP 3. Knowing the parameters of the bubble geometry allows calculation of the water volumes above the bubble, and the pressure p_a , using Eqns (15) through (18), and (20).

$$V_{w1} = \pi(1.3 - 1.3) \left[10 - \frac{1}{24}(3(10)^2 + 3(10)^2 + 4(1.3 - 1.3)^2)\right] = 0$$

$$V_{w2} = \pi(1.3 - 1.3)(2.11)(10 + 2.11) = 0$$

Note that in this case, since $n=H$, it makes sense that $V_{w1} = V_{w2} = 0$.

$$V_{w3} = 2\pi \left[\left(\frac{10}{2} + 2.11\right) - \frac{2.11}{3}\right] \left(\frac{2.11 \times 1.3}{2}\right) = 55.2 \text{ m}^3$$

$$V_{w4} = \pi \left(\frac{1.3 \times 2.11}{6}\right) (10 + 2.11) = 17.4 \text{ m}^3$$

$$p_a = \frac{4 \times 9.81}{\pi(10 + 2 \times 2.11)^2} \times (0 + 0 + 55.2 + 17.4) = 4.48 \text{ kPa}$$

STEP 4. Calculate the geomembrane stress in the upper bubble from Eqn (5).

$$\sigma = \frac{10 \times 4.48}{4 \times 0.0015 \sin \frac{1.658}{2}} = 10,128 \text{ kPa}$$

Given that the goal was to have a stress σ close to 10,000 kPa, the guess of $H = 1.3$ m was a good one. If the calculated value of σ was either too high or too low, the investigator would have to change the value of H and repeat steps 2-4 until the desired value of σ is close to the desired value.

STEP 5. Revise the value of n based on using Eqn (21).

$$n = 1.3 - \frac{4.48}{9.81} = 0.843 \text{ m}$$

This new value of n will change the other calculated geometric values for the bubble, and will require that steps 2-5 be repeated until the values of n and H stabilize, and yield the desired stress level in the geomembrane. In this case a few more iterations on a spreadsheet were adequate to determine that $H_{crit} = 1.44$ m with a value of $n = 0.93$ m.

DISCUSSION OF RESULTS

Using the approach described above, the author has performed these calculations for various size bubbles for a 1.5 mm HDPE geomembrane material to estimate what a maximum allowable underdrain spacing might be to avoid excessive stress on the geomembrane caused by bubbles. In addition to the assumptions being used for the model, this approach also requires the practitioner to define a critical point on the geomembrane material's stress-strain curve. Based on the most conservative, very-slowly strained, multiaxial tests on 1.5 mm HDPE reported by Nobert (1993), the following two states were evaluated for this material: (1) "Ultimate" state where bursting may eventually occur. In this state it assumed that the average strain calculated in the upper portion of the bubble is approximately 12.4% and the stress on a 1.5 mm HDPE geomembrane is approximately 10,000 kPa. This level of strain is achieved when the central angle on the upper portion of the bubble is $\theta = 95$ degrees. (2) Transient "allowable" state, presumed where the strain is 3.7% ($\theta = 53$ degrees), and the corresponding stress is approximately 6,500 kPa.

The results are presented in Table 1. Noteworthy observations include:

1. The smallest bubble that was calculated to achieve potential "burst" conditions for a 1.5 mm HDPE geomembrane has a total base diameter of 8.9 m (29 ft). This could be useful information for designing spacing of underdrain strips, which should be spaced closer than 8.9 m in this case. This bubble would exist in 2.17 m (7.1 ft) of water and only have 0.07 m (0.22 ft) projecting above the water surface, with an internal pressure of only 13 kPa (1.9 psi)

2. The larger the bubble, the lower the critical water depth, and the lower the critical internal pressure.
3. Perhaps one of the most useful take-home messages is how dangerous relatively low bubble pressures can be for the geomembrane. Consider that a 33 m (108 ft) diameter bubble that would potentially be on the verge of bursting would only have an internal pressure of 1.4 kPa (0.2 psi), caused by only 1.15 m (3.8 ft) of water depth. Such a real-world situation is shown in the photo in Figure 3. This means that any underdrain would only require a back-pressure of 0.14 m (5.6 inches) of water column to prevent such a massive bubble from venting or moving. Knowing this it is easy to understand why a flooded underdrain, caused by elevated ground water or a leaking geomembrane, could result in bubbles that do not vent.

Table 1. Solutions for bubble stresses and strains for 1.5 mm HDPE geomembrane.

Assumed dia at POI – c_l (m)	b_l (m)	c_4 (m)	b_4 (m)	H (m)	n (m)	p_a (kPa)	Total dia at base of bubble (m)
“Ultimate” state where bubble strain ϵ_l is set at 12.4% and depth H varied to achieve geomembrane stress σ of approx. 10,000 kPa.							
33.0	7.26	32.7	7.12	1.13	0.99	1.35	36.2
20.0	4.40	19.6	4.17	1.21	0.97	2.26	23.2
10.0	2.20	8.99	1.70	1.44	0.94	4.89	13.0
5.90	1.30	0.88	0.02	2.21	0.94	13.2	8.9
“Allowable” state where bubble strain ϵ_l is set at 3.7% and depth H varied to achieve geomembrane stress σ of approx. 6,500 kPa.							
33.0	3.89	32.8	3.83	0.50	0.45	0.53	35.8
20.0	2.36	19.6	2.26	0.53	0.44	0.88	22.8
10.0	1.18	9.18	0.98	0.62	0.43	1.89	12.7
5.90	0.70	3.86	0.28	0.83	0.41	4.15	8.5



Figure 3. Photo of real-world bubble indicative of calculations presented in the model. Note the people in the photo for scale.

DISCUSSION OF BUBBLE SHAPE AND STRAINS

The equations presented herein are for one geometric condition that reflects the maximum geomembrane stress and strain for a given volume of trapped gas. For the same volume of trapped gas, other values of stress and strain may exist depending on the amount of initial slack in the geomembrane.

There is also a question related to the shape of the bubble in relation to the strain, and how the strain in the geomembrane is distributed over the surface of the bubble. While it is mathematically convenient to calculate strain based on the ratios of computed arc lengths to chord lengths, we find that different regions of the bubble provide different calculated strain results. For example, the ratio of the calculated longitudinal strains for the lower half of the bubble that is below the POI, to the upper half of the bubble that is above the POI, is approximately 1.4, varying slightly depending on which angle θ is chosen. It is not reasonable that there is a step-function in strain levels between the upper and lower halves of the bubble; rather there must be a continuum of strain levels.

Similarly it is not reasonable that there is a step-function of strain level at the limits where the bubble becomes tangent to the pond bottom. While it is reasonable that there could be a strain-gradient at this location, depending on the friction between the geomembrane and the pond bottom, one would expect there to be a continuum rather than a step-function for strain distribution. This situation at the bottom perimeter is one of the differences between a real-world situation, where the bottom conditions are gradual, and a laboratory-testing condition, where the bottom-perimeter condition is typically clamped.

At first glance it would be considered non-conservative to assume that the critical strain in the bubble should be measured as a function of the circular portion of the bubble above the POI, since the calculated strain in the lower portion of the bubble below the POI is greater than the upper portion above the POI. So there is a question of which strain should be used in the calculations to balance the calculated strains with the assumed stresses in the bubble to represent an actual material. At this juncture, for purposes of the model provided in this paper, the author will make some assumptions based on field observations. The author has noted that, particularly with polyethylene geomembranes, but also other geomembrane materials, there is commonly a significant amount of slack in the pond bottom that is evident in the form of wrinkles. The size and frequency of the wrinkles depends on many factors including the type of geomembrane; the temperature difference between the times of deployment, welding, and pond filling; and the interface friction and normal forces between the geomembrane and underlying subgrade (Giroud and Morel, 1992). The author postulates that wrinkles are a source of slack that will provide “body” to the shape of the bubbles, with minimal contribution to geomembrane strain. Each of the wrinkles is also an incipient source of trapped gas (air) below the geomembrane that is the result of installation.

The situation is further complicated by noting that lateral strain distribution may be quite different than longitudinal strain distribution. Bray and Merry (1999), for example, show how the strain is in a biaxial isotropic condition near the pole (top of the bubble), but becomes increasingly anisotropic moving away from the pole down to the base.

Clearly the situation is complicated from a mathematical modeling point of view. Based on the author’s field observations, and for purposes of an expeditious compromise for a first approximation of quantitative calculations of the bubble forces, the author

promotes the simplifying assumption that some amount of geomembrane slack will contribute to the bubble shape without adding to the bubble strain such that the bubble strain can be estimated on the basis of Eqn (2). Certainly other values of strain could be used, and certainly field temperatures have a large influence on the modulus of many materials, which will greatly affect bubble shape and stress. Perhaps more observations and correlations will be made in future works to better define, and put boundaries on, these calculations. One element of field observation that supports the assumption made in this approach is that when real-world bubbles have burst, the failure occurs in the portion of the bubble that is above the water level.

CONCLUSIONS

The analytical approach presented in this paper is intended to provide a first approximation of the quantitative stresses, strains, and pressures in real-world geomembrane bubbles, and seems in line with some real-world experiences that have been witnessed. The methods described in this paper can be currently used in two practical ways. First, observations of bubbles in operating ponds can be evaluated by inputting the estimated bubble diameters and liquid depth to determine if there is cause for concern of damage to the geomembrane. Second, parametric studies can be performed to help design maximum allowable underdrain spacing to de-air potential bubbles. The author notes that for gas-vent underdrains to function properly, they must be completely drained of liquids, and that proper design of underdrains is a separate topic outside the scope of this paper.

Areas identified for further improvements of the analytical model include refinements in defining the geometry of the bubble shape, further studies and measurements of strain distribution in real world bubbles, the influence of initial wrinkles and slack on the stresses and strains in bubbles, and development of representative multiaxial stress-strain curves using appropriate strain rates for different geomembrane materials under different temperatures.

ACKNOWLEDGEMENT

The author would like to acknowledge the industry leadership and service provided by Dr. Robert Koerner, which has inspired the author in the field of geosynthetic engineering for some decades.

REFERENCES

- AISC, Steel Construction Manual, figure for “Properties of Parabola and Ellipse”, American Institute of Steel Construction, , latest edition.
- ASTM D5617, Standard Test Method for Multi-Axial Tension Test for Geosynthetics. Annual Book of ASTM Standards, V04.13. American Society for Testing of Materials, West Conshohocken, PA.
- Bray, J.D, and Merry, S.M. (1999) “A Comparison of the Response of Geosynthetics in the Multiaxial and Uniaxial Test Devices”, *Geosynthetics International*, V6N1, pp. 19-40.
- Coan, J. (2005) “Taking the Mystery Out Of Spiral Curves”, *Evergreen State Surveyor*, a newsletter of the Land Surveyors Association of Washington, Fall 2005. Internet

website:

http://www.alsa.ab.ca/Portals/0/PDF/Member_Resources/Reference_Material/Other/spiral_curves.pdf

- Giroud, J.P. and Goldstein, J.S. (1982) "Geomembrane Liner Design", *Waste Age*, Vol. 13, No. 9, September 1982, pp. 27-30.
- Giroud, J.P. and Morel, N. (1992) "Analysis of Geomembrane Wrinkles." *Journal of Geotextiles and Geomembranes*, V11, Issue 3, pp. 255-276.
- Nobert, J. (1993) "The Use of Multi-Axial Burst Test to Assess the Performance of Geomembranes". *Proceedings of Geosynthetics '93*, Industrial Fabrics Association, International, Roseville, MN, V2, pp. 685-702.